Received: 29 October 2018 | Revised: 5 April 2019 | Accepted: 10 April 2019

DOI: 10.1002/jrs.5617

RESEARCH ARTICLE

WILEY Journal of RAMAN SPECTROSCOPY

Surface-enhanced Raman scattering studies of gold-coated ripple-like nanostructures on iron substrate achieved by femtosecond laser irradiation in water

Chandu Byram | Sree Satya Bharati Moram | Venugopal Rao Soma

Advanced Centre of Research in High Energy Materials (ACRHEM), University of Hyderabad, Hyderabad, India

Correspondence
Venugopal Rao Soma, Advanced Centre of Research in High Energy Materials (ACRHEM), University of Hyderabad, Hyderabad 500046, India.
Email: soma_venu@uohyd.ac.in; soma_venu@yahoo.com

Funding information
DRDO

Abstract

During the past several years, numerous efforts have been accomplished on designing efficient surface-enhanced Raman scattering (SERS) substrates with high sensitivity, good reproducibility, and recyclable nature. However, it still remains a significant challenge to realize all these qualities in a single substrate. We have fabricated ripple-like nanostructures (NSs) on Iron (Fe) substrate using femtosecond (fs) laser irradiation of Fe target in distilled water. These ripple-like structures had periodicities in the range of ~90–190 nm, which was confirmed from the analysis of field emission scanning electron microscope (FESEM) data. We subsequently deposited a thin layer of gold on these ripple-like Fe NSs using thermal evaporation. Later, these coated NSs were effectively utilized as SERS substrates for methylene blue (MB) detection and were found to be sensitive evident from the data obtained at a very low concentration of 500pM. Furthermore, we observed that the SERS signal variations on the substrate were <11.2% indicating the reproducible nature of these substrates. Additionally, we demonstrate that these substrates can be reused (we establish this for three times consecutively) by detecting malachite green (MG) and an explosive molecule (picric acid, PA) followed by the mixture compound (Rhodamine 6G+MB) through employment of simple cleaning procedures. The detected molecular concentrations in terms of masses were found to be 3.2 pg, 36.5 pg, and 23 ng for MB (for a concentration of 500pM), MG (for a concentration of 5nM), and PA (for a concentration of 5μM), respectively. Furthermore, these Fe NSs exhibited superior batch-to-batch reproducibility with a relative standard deviation (RSD) value of ~l4%. The proposed method of fabricating ripple structures as SERS platforms are highly feasible, reliable, and have great potential for on-site detection of several analyte molecules with an easily transportable Raman spectrometer.

KEYWORDS
iron nanostructures, malachite green, methylene blue, Picric Acid, surface enhanced Raman scattering (SERS)

1 | INTRODUCTION

Surface-enhanced Raman scattering (SERS) has emerged as the most promising spectroscopic analytical tool in the research community because of its molecular detection capability with high spectroscopic precision and extraordinary sensitivity.[1] SERS has displayed plenty of applications in a wide range of areas including explosive detection,[2–6] food analysis,[7,8] biosensing,[9] and so on. In SERS, several orders of increment in Raman signals of adsorbed molecules can be observed due to the localized surface plasmons of roughened metal nanostructures (NSs)/nanoparticles (NPs), regarded as electromagnetic enhancement.[10] Besides this, chemical enhancement also plays a minor role in the SERS intensities enhancement, which is attributed to the charge transfer between the analyte molecule and metal NS.[10,11] Giant enhancements in SERS signals can be observed when the analyte molecule is in between two adjacent NPs/NSs (separated by few nm distances), generally referred to as hotspots. During the past few years, intense efforts have been directed towards fabricating efficient SERS substrates with high sensitivity, high reproducibility, long-term stability, and low cost but several efforts are on to achieve all these qualities in a single substrate.[12–15] In this regard, several micro/nanofabrication techniques were investigated for the preparation of SERS substrates such as nanolithography, chemical deposition, self-assembly, and ultrafast laser ablation in liquids (ULAL) techniques.[15–18] Among these, ULAL is a viable and straightforward approach to fabricate novel NPs/NSs with diverse morphologies in a single step, and it has several advantages over the conventional techniques, especially regarding controllability and repeatability.[17] Notably, the NPs/NSs morphology can be altered by tuning the various laser parameters such as pulse width, laser power, scan rate, and the surrounding media. More recently, various research groups, including ours, have demonstrated the fabrication of NPs/NSs in different environments using laser ablation and the SERS measurements conducted by utilizing them.[19–21] Mostly, the laser fabricated NSs made of silver (Ag) and gold (Au) targets and are frequently tested as SERS platforms because of its intriguing plasmonic properties in the visible range.[16,21] Other materials such as transition metals, semiconductors, and magnetic materials are also examined as SERS substrates after deposition of Ag or Au film/NPs (up to few nm).[22–26] Wang et al. fabricated nanoripples and microcones structures on the silicon (Si) substrate using femtosecond (fs) laser ablation and used them as SERS substrates after the Ag film deposition.[24] Yang et al. demonstrated the 4-methyl benzenethiol detection using Si microsquare arrays fabricated by nanosecond laser ablation.[22] Among the other materials, iron (Fe) nanomaterials have found enormous potential bridging from biomedicine to catalysis,[27] magnetic devices,[28] and SERS[29] due to their spectacular properties like physical, chemical, and biocompatibility.[30] Regarding the current developments in SERS technique, a novel approach of combining magnetic materials with plasmonic metals have been introduced by a few research groups recently.[31–34] The advantage of magneto-plasmonic materials is used to separate and detect various multiple analytes like aromatic pollutants, biomarkers, and toxic molecules.[32,33,35] Amendola et al. demonstrated the utility of Au–Fe alloy NPs in SERS and Magnetic Resonance Imaging/Computed tomography imaging.[36] Muniz-Miranda et al. reported the SERS activity of Ag–Fe NPs obtained by two-step laser ablation.[37] However, these NPs achieved from the irradiation of alloy (Au–Fe/Ag–Fe) targets, and cost wise, they are very expensive. Moreover, the NPs-based SERS substrates often caused the problems regarding particle stability, signal homogeneity, controllability, and the nonuniform distribution of hotspots over the large areas. To overcome the disadvantages from the NPs-based SERS susbstrates, a few research groups have demonstrated the fabrication of solid support-based SERS substrates using fs laser ablation of bulk targets in various environments.[19–21] These approaches allow us to fabricate large-area NSs (few cm^2 to few $inches^2$) with distinct morphologies such as periodic gratings/ripples/groves and three-dimensional structures in a variety of materials.[38–40] Especially, laser-induced periodic surface structures (LIPSS)/ripple-like surface structures have found potential applications in numerous fields, but only a few studies have demonstrated the utility of LIPSS and/or ripple-like structures in SERS-based identification of different probe/hazardous molecules.[12,41–43] The periodic/ripple-like structures could play a vital role in SERS-based detection because these structures enable the excitation of the surface plasmon polaritons (SPPs). The SPP supported structure can provide the homogenous electric field distribution over the surface. Therefore, the large area electromagnetic field enhancement occurs at local plasmon-related regions due to the excitation and propagation of surface plasmons.[44,45] Among some of the significant earlier attempts, Buividas et al. demonstrated fabrication of ripple structures on sapphire (Al_2O_3) achieved using fs laser ablation. The laser pulses in their case were focused with a microscope objective lens (N.A 0.7).[43] Further, those ripple structures were coated with Ag/Au (thickness 20-400 nm) and were subsequently utilized for SERS studies of thiophenol (5mM). They observed superior SERS activity of Au/Ag metal-coated ripple structures while detecting thiophenol in comparison with the commercially available substrates (e.g.,

Klarite). They have claimed that the observed superior enhancement in the Raman signal obtained from those metal-coated ripple structures could be attributed to the Au film roughness, surface area as well as the propagation and scattering of SPPs. However, they did not provide any evidence for the contribution of SPPs to the SERS signal. Rebollar et al. reported the SERS performance of Au-coated poly (trimethylene terephthalate) periodic structures obtained with laser irradiation and noticed the substantially larger SERS signals than the Au sputtered flat surface.[41] Barmina et al. recently demonstrated superior SERS activity as well as information storage capacity of laser generated Ni NSs after depositing Au on them.[46] Chang et al. have recently compared the R6G SERS intensities obtained from ripple-like structures and untreated Ag substrate.[42] However, there are no reports on the utility of Fe ripple-like structures obtained using fs LAL for detection of dyes/explosives using the SERS technique.

Herein, we propose a simple and cost-effective approach of fabricating ripple-like structures on the Fe surface through fs laser irradiation of Fe target in the liquid. Fe is widely available and relatively cost-effective (when compared with either Ag or Au) and has wide range of applications in diverse fields. Our main motive is to test the SERS capacity by utilizing the laser-fabricated Fe NSs with metal plating instead of fabricating the magneto-plasmonic NSs from the bulk bimetallic targets. This method is simple and needs lesser time to achieve large area NSs in comparison with the aforementioned approaches. The laser-irradiated Fe NSs can be utilized for SERS studies after deposition of small amount of Au/Ag, which provides feasibility to prepare low-cost substrates by reducing the needed noble metal quantity. For the first time to the best of our knowledge, we report here the utility of gold-coated ripple-like Fe NSs for SERS-based molecular detection. We anticipate that the ripple-like NSs in conjunction with Au coating to generate higher number of hotspots over large areas. Consequently, they are expected to offer superior reproducibility and high sensitivity in the SERS measurements of different analyte molecules. Herein, we demonstrate that these substrates can be recycled/reused (we demonstrate it for three times) without the loss of any significant SERS performance.

2 | EXPERIMENTAL SECTION

2.1 | Synthesis and characterization of iron NSs

To fabricate the NSs, a Ti: sapphire fs laser system (LIBRA, M/s Coherent) delivering ~50 fs pulses at 1-kHz repetition rate, and a central wavelength of 800 nm was utilized for irradiation. The schematic of the NSs fabrication followed by their application in SERS studies is depicted in Figure 1. Initially, iron (Fe) plate (99.99%, Alfa-Aeser) of dimensions 1 cm × cm^2 was cleaned with acetone and water in the ultrasonic bath for 10 min. The Fe plate was fixed at the bottom of the glass cell then filled with 5 ml of distilled water, and the estimated liquid height was ~6 mm from the target surface. The laser beam was impinging normally on to the Fe surface through the plano-convex lens of 100-mm focal length, and the glass cell was mounted on a computer-controlled X-Y stages. The NSs were fabricated in distilled water using three different scanning speeds of 0.25, 0.5, and 1 mm/s with adjacent scanning line interval of 60 μm, and the total scanning area on the Fe surface is ~5 mm^2. In these experiments, the employed input pulse energy was ~150 μJ, which was easily adjusted by a half wave plate and Brewster polarizer combination. To avoid any ambiguity, the fabricated NSs were named as FeDNS1, FeDNS2, and FeDNS3 for the scanning speeds of 0.25, 0.5, and 1 mm/s, respectively. After laser processing, the structural changes in the samples were examined by field emission scanning electron microscope (FESEM, Carl Zeiss) operated at 30 kV, and elemental mapping was conducted by energy dispersive X-ray spectroscopy.

2.2 | Material and chemicals

Iron (99.99%, Alfa-Aeser), methylene blue (MB), malachite green (MG), Rhodamine 6G (R6G), and methanol were purchased from Sigma-Aldrich and utilized without further purification.

2.3 | SERS samples preparation and measurements using Fe NSs

MB (dissolved in methanol), MG (distilled water), and R6G (methanol) were prepared in the concentration ranges from 10^{-1} M-10^{-10} M. Prior to the SER measurements, gold film (20 nm) was sputtered on the NSs using thermal evaporation technique, and the thickness was measured using surface profilometer (Ambios, XP 200). Later, 20-μl solution of the analyte molecule was dripped onto the NSs and dried at room temperature. A portable Raman spectrometer (M/s B&W Tek, USA) utilizing a pump laser with wavelength of 785 nm was utilized in all Raman measurements. An integration time of 5 s was used for all the SERS measurements.

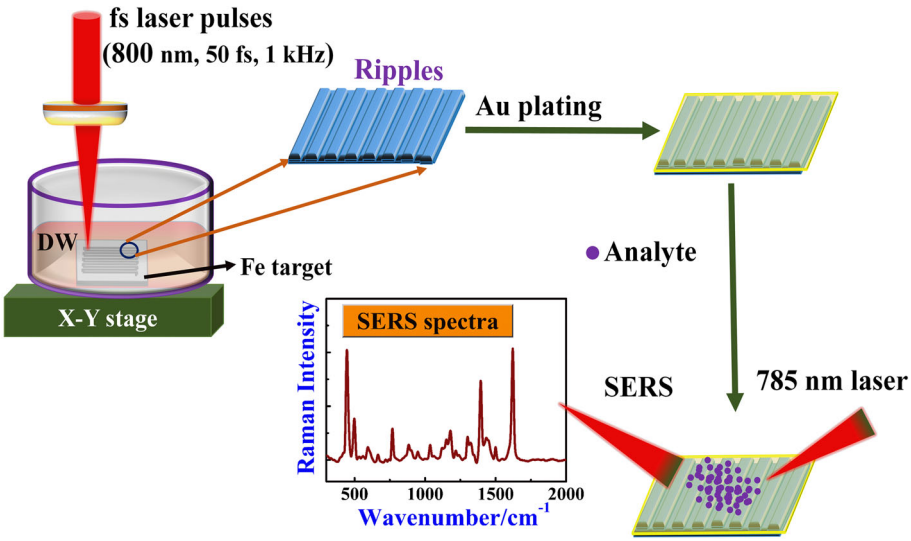

FIGURE 1 Schematic illustrates the proposed surface-enhanced Raman scattering substrates fabrication using liquid assisted femtosecond laser ablation of Fe followed by gold coating and the surface-enhanced Raman scattering studies [Colour figure can be viewed at wileyonlinelibrary.com]

3 | RESULTS AND DISCUSSIONS

Ultrafast ablation of solid materials in liquid has specific advantages when compared with ablation in air/vacuum. In the vicinity of ambient fluid, laser-induced thermal damages can be significantly reduced due to the cooling and heat sink provided by the surrounding liquid. Furthermore, generated bubbles from the evaporated liquid remove the deposited ablation debris on target material, which leads to the increase of ablation depth.[47,48] Thus, liquid-assisted ablation was introduced to fabricate precise micro/nanostructures on different materials. Moreover, both the NPs and NSs can be fabricated in a single exposure/experiment using this ULAL technique. In the current study, fs laser-induced ripple-like structures of different periodicities were obtained on Fe surface in the presence of liquid environment by simply altering the laser scanning conditions. The lower and higher magnification FESEM images of the morphological variations in fs laser treated portions on Fe surface are displayed in Figure 2 (a1, a2; b1,b2; and c1, c2) for FeDNS1, FeDNS2, and FeDNS3, respectively. In all the irradiated conditions, ripples were noticed with different periodicities. The direction of the produced ripples was perpendicular to the input polarization direction.

We observed that at a lower scanning speed of 0.25 mm/s, the ripples are self-organized with periodicities in the range of ~106–175 nm (data is shown in Figure 2a1,a2 and named as FeDNS1). Figure S1a,b (supporting information) illustrates recorded SEM mage and energy dispersive X-ray spectra on FeDNS1 after Au coating, which revealed the presence of Au on the substrate. However, the SEM image looks slightly different, which could be due to the fact that the captured image might be at a different location on the FeDNS1 (before and after Au sputtering). In the case of FeDNS2 substrate, ripples with periodicities of ~95–135 nm were observed, and further, we noticed a number of NPs with arbitrary shapes on top of the NS, as shown in Figure 2b1,b2. While at a higher scanning speed of 1 mm/s (named as FeDNS3), ripples with periodicities of ~135–190 nm and a smaller sized NPs were observed in the gaps of the ripples as depicted in Figure 2c1,c2. The observed nano-droplets on top of the ripples can be attributed to the formed molten layer on the Fe surface during the ablation. This molten layer rapidly solidifies and is re-deposited back on to the target material in the form of particles.[49,50] The average ripple periodicities are estimated by considering more than three SEM images in each case, and the calculated periodicities are 143 ± 24 nm, 120 ± 16 nm, and 152 ± 24 nm for FeDNS1, FeDNS2, and FeDNS3, respectively. These are calculated using the ImageJ software available commercially. In this study, the estimated ripple periodicities are much smaller than the incident light, which can be treated as high-spatial frequency (HSFL) LIPSS. It is wieldy accepted that HSFL LIPSS could be formed when the ultrafast pulses are used (few ps or fs) in irradiation, and the formation of LIPSS (HSFL) can be explained from the surface plasmon theory as follows: When the multiple laser pulses interact with the target surface, interference could occur between the incident laser pulses and generated surface scattered waves at the metal-dielectric introducing a thermal gradient and, subsequently, a periodic intensity

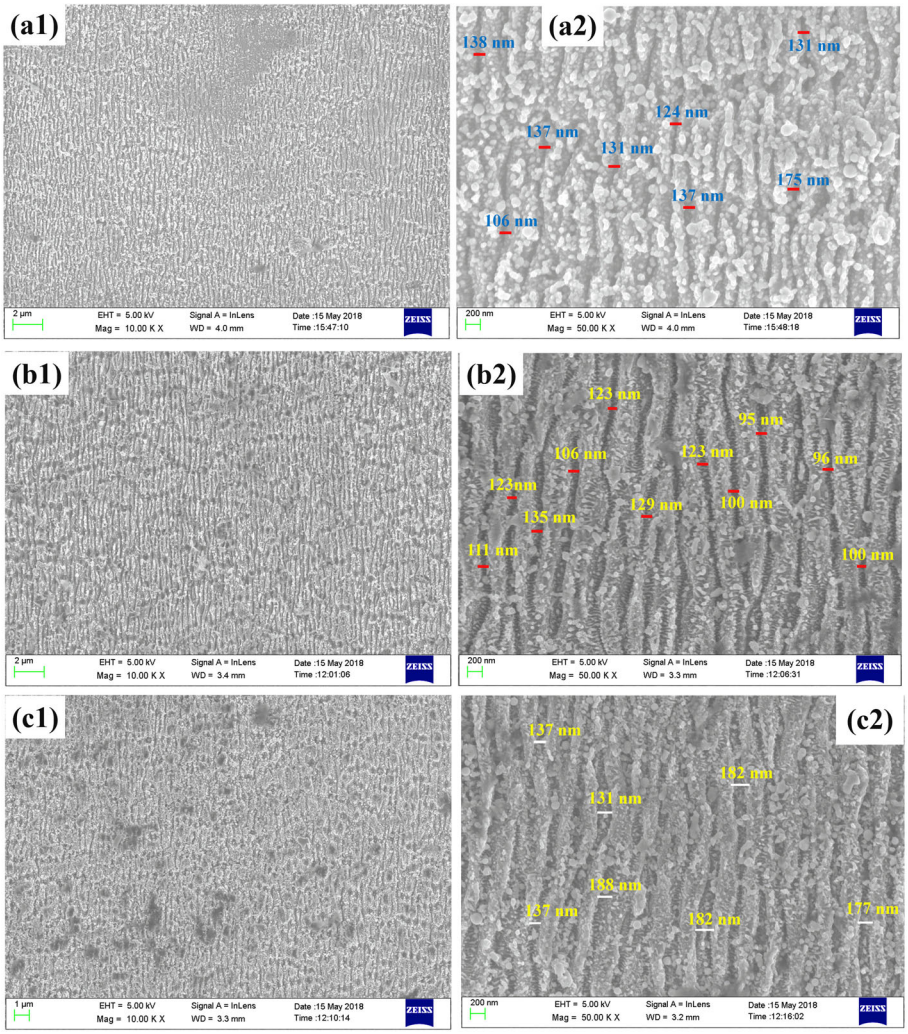

FIGURE 2 Lower and higher magnification [periodicities were labeled in (a2), (b2), (c2)] field emission scanning electron microscope images of FeDNS1 (a1, a2), FeDNS2 (b1, b2), and FeDNS3 (c1, c2) [Colour figure can be viewed at wileyonlinelibrary.com]

variation over the target surface. Due to the thermal gradient, induced thermo-capillary forces will transport the melted material from the hotter region to colder region, resulting in the periodical NSs with a self-organization process.[51,52] However, the underlying exact mechanism in HSFL LIPSS formation on various materials is still debated. Similar to our study, Liu et al. demonstrated the formation of HSFL (period [Λ] of ~150–230 nm), and LSFL (Λ of ~500–640 nm) LIPSS on Fe films using fs laser ablation studies in air.[53] However, the obtained ripple periodicities in our present study are not completely uniform, which could be attributed to the effect of used different laser processing conditions (laser fluence, pulse numbers) and also the effect surrounding liquid. Gnilitskyi et al. investigated the formation of highly regular LIPSS on various metals (Al, Ti, Cu, Mo, Au, and steel) by changing the laser parameter (laser pulse fluences, scanning parameter, etc.) in ambient air.[54] They achieved the regular LIPSS only on Ti, Mo, and steel among the others (Al, Cu, and Au), which might be due to the need of specific laser processing conditions (laser wavelength, scanning conditions, etc.) for particular metal. Guo et al. have also studied in detail the LIPSS formation on various metals (Cu, Ag, and Au) and noticed regular LIPSS patterns on Cu in comparison with Ag and Au.[55] The periodic structures formation depends on several factors including (a) number of incident pulses (b) focusing geometry and conditions (c) input energy and (d) surrounding atmosphere etc.

3.1 | SERS Activity of the Fe NSs

Before conducting the SERS measurements, a 20-nm Au film was coated on to the fabricated NSs using thermal evaporation technique. The coated Au film generates surface plasmons on the NSs by providing conduction electrons, which is crucial for an active SERS substrate.

The recorded Raman spectra on plain Au-coated, laser-treated (before and after Au deposition) Fe surface are presented in Figure S2 (curves [i–iv]). The data presented in Figure S2 revealed that there were no impurities found on the substrate. The NSs SERS activity was evaluated using MB as a probe molecule. Figure 3a represents the recorded Raman spectra of MB (0.1 M) on the plain Fe surface (without Au coating), and the major modes were labeled in the inset. The high-intensity Raman modes observed at 446 and 1620 cm^{-1} can be ascribed to the skeletal deformation of C-N-C and C-C ring stretching. The lower intensity modes noticed at 499, 769, and 1,393 cm^{-1} are assigned to the C-N-C skeletal deformation, C-H in-plane bending, and C-N symmetric stretching, which are in accordance with the earlier published results.[21,56,57] Figure 3b presents the recorded SERS spectra of MB (5nM) from the FeDNS1, FeDNS2, and FeDNS3 substrates, and the noticed spectral modes are slightly shifted, which can possibly be due to the orientation of probe molecule on the NSs. The enhancement factors (EFs) were estimated by considering the high-intensity mode of MB (1,618 cm^{-1}) observed from the SERS substrate as well as from the plain substrate.

The estimated EFs from the FeDNS1, FeDNS2, and FeDNS3 are 3.4×10^6, 5.3×10^6, and 2.4×10^6, respectively. Among the other substrates, higher SERS EF was observed for FeDNS2 substrate, and reasons can be explained as follows. During the film deposition, Au NPs might be distributed over the ripple-like structures, which could decrease the spacing between the ripples leading to the formation of a higher number of hotspots.[58,59] Due to the generated hotspots between the decorated NPs and periodic NSs, the local electric field will be enhanced significantly and, therefore, results in a higher SERS signal.[59] We also believe that there could be an effect of ripple period on the observed SERS enhancements in the present case. However, with limited data available, we cannot conclude and comment on this at this point of time. Kalachyova et al.[45,60–62] recently demonstrated the SERS-based detection of Rh6G and other molecules using laser-fabricated periodic structures on various polymers coated with Au/Ag and observed the superior and reproducible SERS signals with the help of SPP supported structures (gratings and/or periodic structures). They clearly demonstrated the effect of periodicity of the gratings on the SERS signals for different materials including Ag. Further detailed experiments are needed to highlight the contribution of periodicity on the SERS enhancements. The existing literature has demonstrated that the periodic structures-based sensors achieved from various chemical approaches acted as efficient SERS platforms regarding sensitivity, selectivity, and signal uniformity.[63–66] Herein, Au-coated ripple structures have shown the superior EFs to some of earlier published

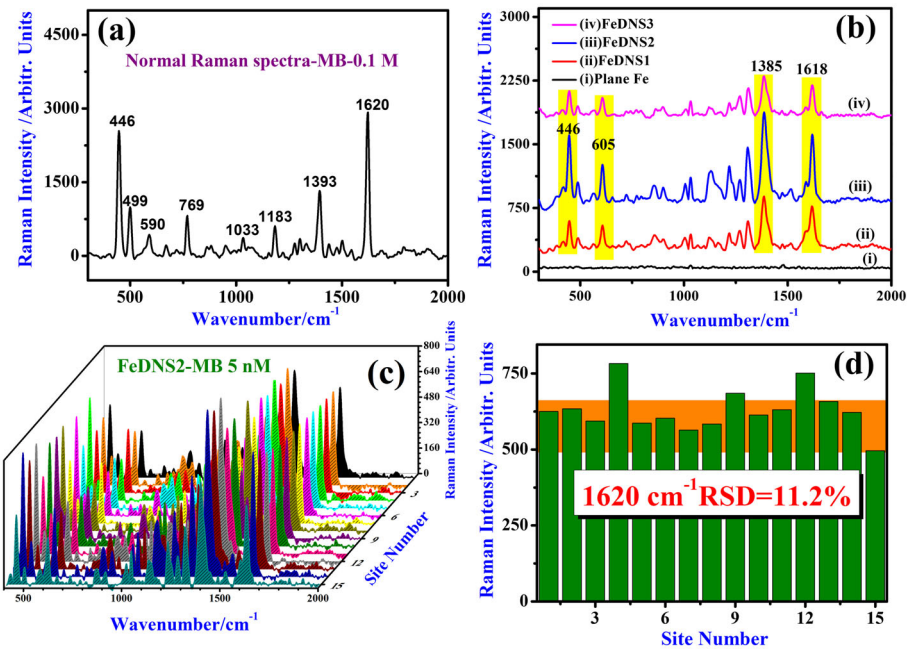

FIGURE 3 (a) Normal Raman spectra of MB (0.1M) recorded on plain Fe surface (b) surface-enhanced Raman scattering spectra of MB (5nM) recorded on (i) plain Fe, (ii) FeDNS1, (iii) FeDNS2, and (iv) FeDNS3 substrates after Au deposition. (c) 3D surface-enhanced Raman scattering spectra of methylene blue (5nM) collected from randomly selected 15 sites on FeDNS2 substrate (c) calculated relative standard deviation value for the 1,618 cm^{-1} methylene blue peak intensity [Colour figure can be viewed at wileyonlinelibrary.com]

results, and the fabricated methodology in the present study is simple, viable, and could be cost-effective when compared with the chemical approaches.

Reproducibility is detrimental for the practical use of SERS substrates. Therefore, to examine the FeDNS2 substrate homogeneity, the Raman spectra were acquired at randomly selected 15 sites, and the data are presented in Figure 3c,d. It is apparent from the data that the substrate exhibited good reproducibility with a relative standard deviation (RSD) of 11.2% for the SERS intensity of MB (10^{-9}M) 1,618 cm^{-1} peak. FeDNS1 and FeDNS3 substrates reproducibility measurements with calculated RSD values are presented in Figure S3. For comparison purpose, MB (5nM) signals recorded from Au-coated plain Fe surface (presented as black/bottom curve in Figure 3b) did not demonstrate any of the MB modes. Further, Au film effect on SERS intensities was investigated by recording the higher concentration of MB (10^{-6}M) spectra on Au-coated plain and laser-treated FeDNS2 substrate. The SERS data of MB for both of these substrates are presented in Figure 4. In this study, laser-treated Fe surface exhibited ~76 times higher SERS enhancement than the untreated surface (after Au deposition), which is much higher than the earlier reported value.[41] The observed significant SERS enhancement could possibly have contributions from the roughness of the Au film as well as localized and propagating SPPs originating from these ripple-like structures. However, detailed polarization spectroscopic studies will confirm this and mandate further detailed investigations.[43–45] In an earlier study, Chang et al. demonstrated that the Ag periodic structures exhibited ~15 times higher SERS signals than the plain Ag surface.[42] Earlier, we demonstrated the pure Au NSs SERS activity[21] and found EFs of ~1.5×10^{6}, but in the present case, we could achieve four times better enhancement with higher sensitivity. Additionally, a smaller quantity (5 mg) of Au was used to coat the Fe NSs in this case, and consequently, the cost of SERS substrate has significantly reduced. It is important to mention that the morphology of laser-treated surface plays a significant role in observing higher SERS enhancements with the coated Ag/Au film. Table S1 summarizes and provides a comparison of the several detected analyte molecules using Au/Ag-coated laser fabricated NSs.

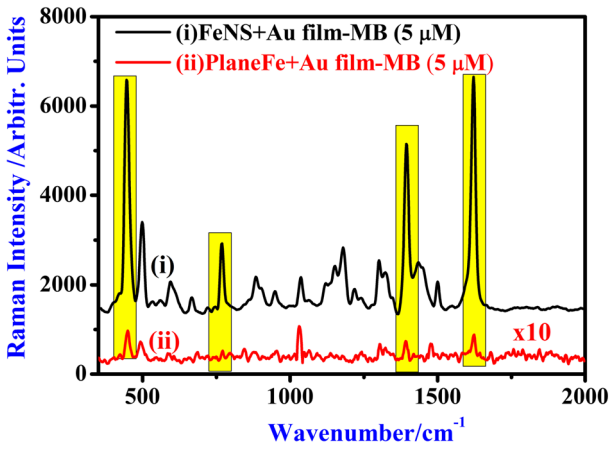

FIGURE 4 Recorded surface-enhanced Raman scattering spectra of methylene blue (5μM) on Au-coated (i) laser-treated (FeDNS2) and (ii) untreated Fe surface. Major modes of methylene blue are highlighted with yellow color [Colour figure can be viewed at wileyonlinelibrary.com]

Further, the detection sensitivity of FeDNS2 substrate was investigated by collecting the Raman signal of MB with various concentrations ranging from 10^{-6}M to 10^{-10}M. Figure 5a,b depicts the concentration spectra of MB (10^{-6}M–10^{-10}M) and their corresponding linear calibration curve for the SERS intensity of 1,618 cm^{-1} mode with respect to the concentration. The linear fitting curve displays the correlation coefficient of R^2 of ~0.92 (Figure 5 b). Even at 500pM, most of the MB characteristic modes are distinguishable, which revealed the high sensitivity of FeDNS2 substrate. Here, the reported detection limit is superior to some of the earlier reported SERS substrates

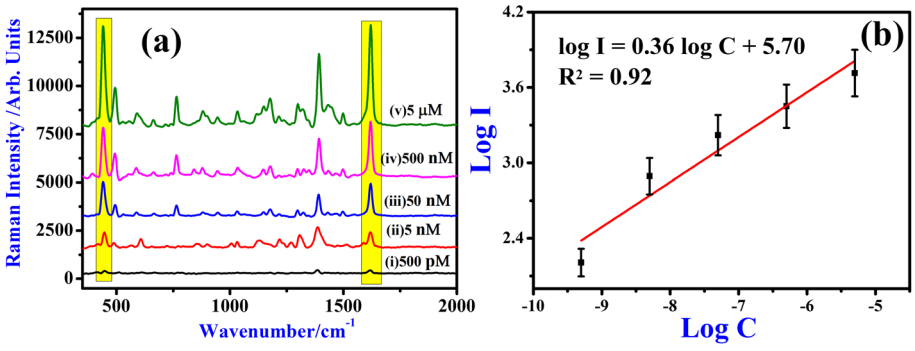

FIGURE 5 (a) Surface-enhanced Raman scattering spectra of methylene blue with different concentrations [(i) 500pM, (ii) 5nM, (iii) 50nM, (v) 500nM, (iv) 5 μM] recorded on FeDNS2 (b) linear calibration curve by considering the intensities of 1,618 cm^{-1} mode with respect to the concentration of methylene blue. [Colour figure can be viewed at wileyonlinelibrary.com]

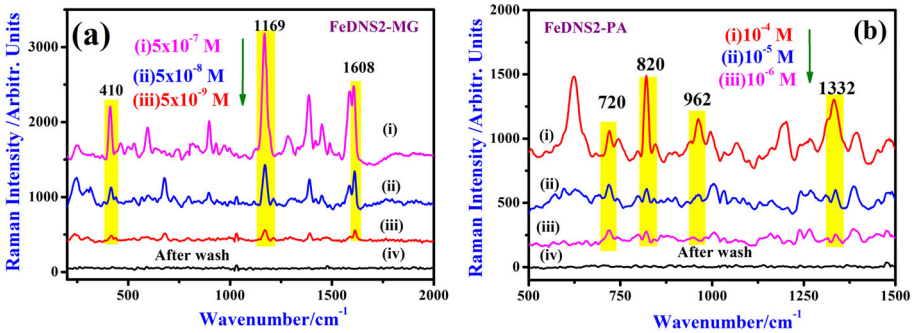

FIGURE 6 (a) Surface-enhanced Raman scattering spectra of malachite green [(i) 500nM, (ii) 50nM, (iii) 5nM] (b) surface-enhanced Raman scattering spectra of picric acid [(i) 10^{-4}M, (ii) 10^{-5}M, (iii) 10^{-6}M] recorded from FeDNS2 substrate. Inset of (a) and (b) black one (Curve iv) represents the spectra recorded on FeDNS2 substrate after cleaning [Colour figure can be viewed at wileyonlinelibrary.com]

fabricated with laser irradiation.[21,23,41] In addition to the sensitivity and reproducibility, the substrate-to-substrate reproducibility is also a crucial factor for SERS platforms in real-world applications because most of the substrates lack the batch-to-batch repeatability. To inspect the substrate-to-substrate SERS intensity variation, four substrates (FeDNS2) were fabricated independently at similar conditions, and then the MB (5nM) SERS data were collected, and the data are presented in Figure S4a. The SERS intensity (1,618 cm^{-1} peak) variation from the substrate to substrate is estimated to be ~14% (inset of Figure S4a) revealing the decent batch-to-batch reproducibility of these SERS substrates. Furthermore, each substrate exhibited an excellent reproducibility with the RSD values of <13% for the intensity of 1,618 cm^{-1} MB (5nM) peak collected at five different spots on each substrate (data are shown in Figure S4b).

Due to the higher sensitivity of FeDNS2, this substrate was recycled for the detection of other molecules following appropriate cleaning procedures. Briefly, the substrate was immersed in methanol for 30 min to dissolve the MB then sonicated with water and acetone in the ultrasonic bath for 10 min. After washing the substrate, SERS signals were acquired to check whether MB was completely washed out or not. As presented in Figure 6a (Curve iv), no distinct Raman peaks of MB were noticed on the FeDNS2 substrate after cleaning. Then, the FeDNS2 substrate was treated with another aromatic dye molecule MG, which is commonly used dye in paper, textile, and fisheries industries. MG is banned in most of the countries because of its negative impacts on DNA-related damages, and also, it is poisonous to many aquatic animals. Therefore, there is an urgent need for accurate and sensitive detection technique for MG at lower concentrations. Figure 6a depicts the MG concentration spectra varying from 10^{-7}M to10^{-9}M, and the prominent modes were observed at 410 cm^{-1}, 1,169 cm^{-1}, and 1,608 cm^{-1}, which are attributed to the out-of-plane vibration of phenyl-C-phenyl, in-plane bending of C-H, and C-C ring stretching, respectively.[67] After washing the substrate, none of the Raman peaks of MG were found and is evident from the data presented in Figure 6b (Curve iv). Subsequently, we performed the SERS measurements with an explosive molecule of picric acid (PA) using the same substrate

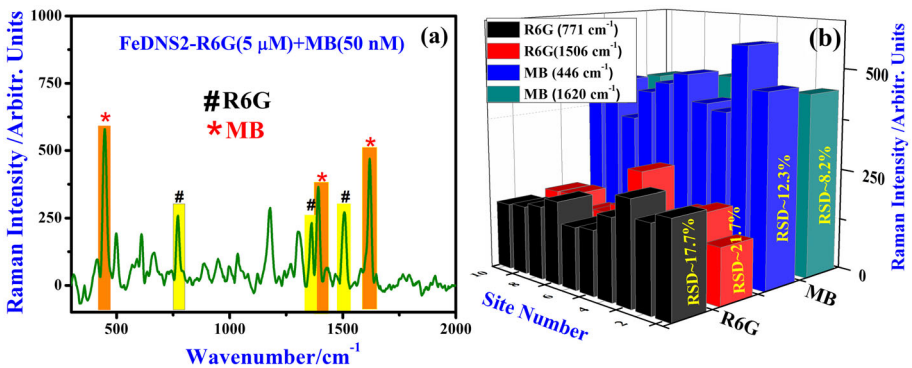

FIGURE 7 (a) Surface-enhanced Raman scattering spectra of mixture (R6G [5μM]), peaks labeled with # + methylene blue (50nM), peaks labelled with *] (b) measured surface-enhanced Raman scattering intensity for the prominent modes of both compounds (R6G [771, 1,506 cm $^{-1}$] and methylene blue [446, 1,620 cm^{-1}]) in mixed spectra collected at 10 different spots on FeDNS2 substrate [Colour figure can be viewed at wileyonlinelibrary.com]

after second cleaning (using earlier mentioned procedure). PA is a well-known explosive and is widely utilized in pesticides, manufacturing of acid dyes, photographic drugs, etc. PA also causes the environment pollution through water and soil. Later, various concentrations of PA (ranging from 10^{-4}M to 10^{-6}M) were used to record the SERS spectra on FeDNS2 substrate, and the data are presented in Figure 6b. PA characteristic modes are located at 820, 962, and 1,332 cm^{-1}, which are associated with the C-H bending, ring breathing, and NO_2 symmetric stretching, respectively. The observed modes are in good agreement with the published literature.[68,69] The detected PA concentration levels are lower owing to its smaller Raman scattering cross-section compared with the dye molecules. Further, the orientation of the analyte molecule on the substrate also determines the SERS enhancement. Additionally, the SERS capability of FeDNS2 substrate was again tested with mixture sample containing R6G and MB in equal volumes (1:1). Figure 7a represents the SERS spectra of the mixture (R6G [5μM] + MB [50nM]), and the prominent modes of R6G (peaks are shown with the # symbol) and MB (peaks represented with * symbol) are highlighted with orange and yellow boxes in the inset. In Figure 7b, bar chat indicates the SERS intensity variation with the position for the mixed sample recorded at 10 different places on FeDNS2 substrate.

The RSD values for the most intense peaks of R6G (771 and 1,506 cm^{-1}) and MB (446 and 1,620 cm^{-1}) are found to be <22% revealing the good reproducibility nature of the as-fabricated SERS substrates even after usage for three times. The observed SERS peak intensities for R6G modes are found to be lower than the MB peak intensities in mixed spectra, which could be due the (a) interaction of analyte (mixture) with NSs (b) the excitation wavelength (785 nm in present case) used being nearer to the absorption maxima of MB (~650 nm)[56] than for R6G (~530 nm) (c) Raman cross-section of analyte molecules at used excitation source (785 nm in the present study). To comprehend the complete picture of SERS intensity variations for the mixed analyte, one has to perform the SERS measurements with different Raman excitation sources. We are working on extending these investigations further. Our present study is mainly focused on identification of the mixed analytes using the fabricated NSs, which will be later extended to detect explosive mixtures because most of the explosives are not transported in single phase.

Thus far, most of the reported Ag–Fe/Au–Fe SERS substrates are NPs-based substrates, which have a deficiency in signal uniformity due to the irregular arrangement of hotspots. However, in the present study, the multiple utility of Fe ripple structures was demonstrated as SERS sensors with higher uniformity over the large area (5 mm^2). The observed enhancements (EFs of ~10^7) clearly suggest that these structures can be efficaciously utilized as SERS sensors (e.g., for environmental monitoring applications). Apart from this, we firmly believe that these Au-coated Fe ripple structures can also be utilized for information storage devices. Furthermore, the efficacy (for SERS studies) of these structures could be improved by (a) obtaining truly periodic three-dimensional structures of different sizes supporting the strong SPP (b) combine NPs (obtained by ULAL or chemical methods) and these NSs, which has been a proven methodology to improve the SERS enhancements,[20,70] (c) achieving hybrid NSs of Ag/Au on Fe NSs simply by ablating the Fe target in either $AgNO_3$ or $HAuCl_4$.

4 | CONCLUSIONS

In summary, laser-induced ripple-like structures on Fe substrate were obtained using liquid assisted fs irradiation, and the obtained ripple periodicities were lies in the range of ~90–190 nm. After the Au film deposition, the fabricated periodic Fe NSs used as SERS sensors for MB (10^{-10}M) detection, and we could find the higher enhancements with better reproducibility (RSD ~11.2%) for FeDNS2 substrate. Besides, the Au-coated ripple-like Fe NSs have significantly enhanced the SERS signals (~76 times higher) than the Au-coated plain Fe surface. Furthermore, the FeDNS2 substrate was reused for detecting MG, PA, and the mixture compound (R6G +MB) after cleaning following a simple protocol. Even after reuse, the optimized FeDNS2 substrate exhibited improved detection limits as low as 10^{-9}M (which corresponds to a weight of 36.5 pg), 10^{-6}M (which corresponds to a weight of 23 ng) for MG and PA, respectively, without losing its SERS activity. Additionally, the proposed SERS substrates have demonstrated a higher batch-to-batch reproducibility with an RSD value of ~14%. The presented strategy of fabricating ripple-like structures and their utility as a SERS sensor can pave a new way for multiple molecules detection in real-field applications using a simple, portable Raman instrument.

ACKNOWLEDGEMENTS

The authors thank DRDO, India for continuous financial support. The authors also thank the Mr. D. Borgohain, School of Engineering Sciences & Technology, University of Hyderabad for his help in film deposition experiments. Authors thank School of Physics, University of Hyderabad for support in FESEM imaging and Centre for Nanotechnology, University of Hyderabad for film deposition.

ORCID

Venugopal Rao Soma https://orcid.org/0000-0001-5361-7256

REFERENCES

[1] M. Moskovits, *Rev. Mod. Phys.* **1985**, *57*, 783.

[2] T. Liyanage, A. Rael, S. Shaffer, S. Zaidi, J. V. Goodpaster, R. Sardar, *Analyst* **2018**, *143*, 2012.

[3] C. Zhang, K. Wang, D. Han, Q. Pang, *Spectrochim. Acta. Part A* **2014**, *122*, 387.

[4] S. Botti, L. Cantarini, A. Palucci, *J. Raman Spectrosc.* **2010**, *41*, 866.

[5] S. Botti, S. Almaviva, L. Cantarini, A. Palucci, A. Puiu, A. Rufoloni, *J. Raman Spectrosc.* **2013**, *44*, 463.

[6] A. Hakonen, P. O. Andersson, M. S. Schmidt, T. Rindzevicius, M. Käll, *Anal. Chim. Acta* **2015**, *893*, 1.

[7] X. Liang, X. J. Zhang, T. T. You, N. Yang, G. S. Wang, P. G. Yin, *J. Raman Spectrosc.* **2018**, *49*, 245.

[8] J. Jiang, S. Zou, L. Ma, S. Wang, J. Liao, Z. Zhang, *ACS Appl. Mater. Interfaces* **2018**, *10*, 9129.

[9] E. Petryayeva, U. J. Krull, *Anal. Chim. Acta* **2011**, *706*, 8.

[10] A. Campion, P. Kambhampati, *Chem. Soc. Rev.* **1998**, *27*, 241.

[11] A. Campion, J. Ivanecky III, C. Child, M. Foster, *J. Am. Chem. Soc.* **1995**, *117*, 11807.

[12] A. Chou, E. Jaatinen, R. Buividas, G. Seniutinas, S. Juodkazis, E. L. Izake, P. M. Fredericks, *Nanoscale* **2012**, *4*, 7419.

[13] P. Sajanlal, T. Pradeep, *Nanoscale* **2012**, *4*, 3427.

[14] P. M. Fierro-Mercado, S. P. Hernández-Rivera, *Int. J. Spectro.* **2012**, *2012*, 716527.

[15] L. Štolcová, V. Peksa, J. Proška, M. Procházka, *J. Raman Spectrosc.* **2018**, *49*, 499.

[16] S. V. Rao, G. K. Podagatlapalli, S. Hamad, *J. Nanosci. Nanotechnol.* **2014**, *14*, 1364.

[17] D. Zhang, B. Gökce, S. Barcikowski, *Chem. Rev.* **2017**, *117*, 3990.

[18] H. Zhao, W. Hasi, L. Bao, Y. Liu, S. Han, D. Lin, *J. Raman Spectrosc.* **2018**, *49*, 1469.

[19] G. K. Podagatlapalli, S. Hamad, S. V. Rao, *J. Phys. Chem. C* **2015**, *119*, 16972.

[20] C. Byram, V. R. Soma, *Nano-Struct. Nano-Objects* **2017**, *12*, 121.

[21] C. Byram, S. S. B. Moram, A. K. Shaik, V. R. Soma, *Chem. Phys. Lett.* **2017**, *685*, 103.

[22] J. Yang, J. Li, Z. Du, Q. Gong, J. Teng, M. Hong, *Sci. Rep.* **2014**, *4*, 6657.

[23] E. D. Diebold, N. H. Mack, S. K. Doorn, E. Mazur, *Langmuir* **2009**, *25*, 1790.

[24] A. Wang, L. Jiang, X. Li, Q. Xie, B. Li, Z. Wang, K. Du, Y. Lu, *J. Mater. Chem. B* **2017**, *5*, 777.

[25] K. Wu, T. Rindzevicius, M. S. Schmidt, A. H. Thilsted, A. Boisen, *J. Raman Spectrosc.* **2017**, *48*, 1808.

[26] S. Botti, L. Cantarini, S. Almaviva, A. Puiu, A. Rufoloni, *Chem. Phys. Lett.* **2014**, *592*, 277.

[27] R. Madon, W. Taylor, *J. Catal.* **1981**, *69*, 32.

[28] H. Xia, J. Wang, Y. Tian, Q. D. Chen, X. B. Du, Y. L. Zhang, Y. He, H. B. Sun, *Adv. Mater.* **2010**, *22*, 3204.

[29] L.-P. Wang, Y.-B. Huang, Y.-H. Lai, *Appl. Surf. Sci.* **2018**, *435*, 290.

[30] J. Gao, H. Gu, B. Xu, *Acc. Chem. Res.* **2009**, *42*, 1097.

[31] S. Scaramuzza, D. Badocco, P. Pastore, D. F. Coral, M. B. Fernández van Raap, V. Amendola, *ChemPhysChem* **2017**, *18*, 1026.

[32] C. Yuen, Q. Liu, *Analyst* **2013**, *138*, 6494.

[33] J. Du, C. Jing, *J. Phys. Chem. C* **2011**, *115*, 17829.

[34] V. Amendola, S. Scaramuzza, S. Agnoli, G. Granozzi, M. Meneghetti, G. Campo, V. Bonanni, F. Pineider, C. Sangregorio, P. Ghigna, *Nano Res.* **2015**, *8*, 4007.

[35] X. X. Han, A. M. Schmidt, G. Marten, A. Fischer, I. M. Weidinger, P. Hildebrandt, *ACS Nano* **2013**, *7*, 3212.

[36] V. Amendola, S. Scaramuzza, L. Litti, M. Meneghetti, G. Zuccolotto, A. Rosato, E. Nicolato, P. Marzola, G. Fracasso, C. Anselmi, *Small* **2014**, *10*, 2476.

[37] M. Muniz-Miranda, C. Gellini, E. Giorgetti, G. Margheri, *J. Colloid Interface Sci.* **2017**, *489*, 100.

[38] R. Buividas, M. Mikutis, T. Kudrius, A. Greičius, G. Šlekys, S. Juodkazis, *Lith. J. Phys.* **2012**, *52*.

[39] R. Buividas, S. Rekštytė, M. Malinauskas, S. Juodkazis, *Opt. Mater.Express.* **2013**, *3*, 1674.

[40] K. Sugioka, Y. Cheng, *Appl. Phys. Rev.* **2014**, *1*, 041303.

[41] E. Rebollar, M. Sanz, S. Perez, M. Hernandez, I. Martín-Fabiani, D. R. Rueda, T. A. Ezquerra, C. Domingo, M. Castillejo, *Phys. Chem. Chem. Phys.* **2012**, *14*, 15699.

[42] H.-W. Chang, Y.-C. Tsai, C.-W. Cheng, C.-Y. Lin, Y.-W. Lin, T.-M. Wu, *J. Colloid Interface Sci.* **2011**, *360*, 305.

[43] R. Buividas, P. R. Stoddart, S. Juodkazis, *Ann. Phys.* **2012**, *524*, L5.

[44] F. J. Bezares, J. D. Caldwell, O. Glembocki, R. W. Rendell, M. Feygelson, M. Ukaegbu, R. Kasica, L. Shirey, N. D. Bassim, C. Hosten, *Plasmonics* **2012**, *7*, 143.

[45] Y. Kalachyova, D. Mares, O. Lyutakov, M. Kostejn, L. Lapcak, V. Švorčík, *J. Phys. Chem. C* **2015**, *119*, 9506.

[46] E. V. Barmina, C. Lau Truong, F. Bozon-Verdyura, Z. Levi, A. V. Simakin, G. A. Shafeev, *Quantum Electron.* **2010**, *40*, 346.

[47] R. An, M. D. Hoffman, M. A. Donoghue, A. J. Hunt, S. C. Jacobson, *Opt. Express* **2008**, *16*, 15206.

[48] H. Liu, F. Chen, X. Wang, Q. Yang, H. Bian, J. Si, X. Hou, *Thin Solid Films* **2010**, *518*, 5188.

[49] E. Stratakis, V. Zorba, M. Barberoglou, C. Fotakis, G. Shafeev, *Appl. Surf. Sci.* **2009**, *255*, 5346.

[50] A. De Bonis, T. Lovaglio, A. Galasso, A. Santagata, R. Teghil, *Appl. Surf. Sci.* **2015**, *353*, 433.

[51] J. Sipe, J. F. Young, J. Preston, H. Van Driel, *Phys. Rev. B.* **1983**, *27*, 1141.

[52] J. Bonse, S. Höhm, S. V. Kirner, A. Rosenfeld, J. Krüger, *IEEE J. Sel. Top. Quantum Electron.* **2017**, *23*, 109.

[53] K. Liu, X. Li, C. Xie, K. Wang, Q. Zhou, R. Qiu, *Opt. Laser Technol.* **2017**, *94*, 28.

[54] I. Gnilitskyi, T. J.-Y. Derrien, Y. Levy, N. M. Bulgakova, T. Mocek, L. Orazi, *Sci. Rep.* **2017**, *7*, 8485.

[55] J. Wang, C. Guo, *Appl. Phys. Lett.* **2005**, *87*, 251914.

[56] M. Sree Satya Bharati, C. Byram, V. R. Soma, *Front. Phys.* **2018**, *6*, 28.

[57] J. Anastasopoulos, A. Soto Beobide, A. Manikas, G. Voyiatzis, *J. Raman Spectrosc.* **2017**, *48*, 1762.

[58] C. Zhang, P. Yi, L. Peng, X. Lai, J. Chen, M. Huang, J. Ni, *Sci. Rep.* **2017**, *7*, 39814.

[59] J. Tang, F. S. Ou, H. P. Kuo, M. Hu, W. F. Stickle, Z. Li, R. S. Williams, *Appl. Phys. A.* **2009**, *96*, 793.

[60] Y. Kalachyova, D. Mares, V. Jerabek, K. Zaruba, P. Ulbrich, L. Lapcak, V. Svorcik, O. Lyutakov, *J. Phys. Chem. C* **2016**, *120*, 10569.

[61] Y. Kalachyova, D. Mares, V. Jerabek, P. Ulbrich, L. Lapcak, V. Svorcik, O. Lyutakov, *Phys. Chem. Chem. Phys.* **2017**, *19*, 14761.

[62] Y. Kalachyova, M. Erzina, P. Postnikov, V. Svorcik, O. Lyutakov, *Appl. Surf. Sci.* **2018**, *458*, 95.

[63] C. Farcau, S. Astilean, *J. Mol. Struct.* **2014**, *1073*, 102.

[64] Y. Jin, Y. Wang, M. Chen, X. Xiao, T. Zhang, J. Wang, K. Jiang, S. Fan, Q. Li, *ACS Appl. Mater. Interfaces* **2017**, *9*, 32369.

[65] W. Tao, A. Zhao, H. Sun, Z. Gan, M. Zhang, D. Li, H. Guo, *RSC Adv.* **2014**, *4*, 3487.

[66] J. Beermann, S. M. Novikov, K. Leosson, S. I. Bozhevolnyi, *Opt. Express* **2009**, *17*, 12698.

[67] Y. Zhao, Y. Tian, P. Ma, A. Yu, H. Zhang, Y. Chen, *Anal. Methods* **2015**, *7*, 8116.

[68] S. S. B. Moram, C. Byram, S. N. Shibu, B. M. Chilukamarri, V. R. Soma, *ACS Omega* **2018**, *3*, 8190.

[69] A. Hakonen, F. Wang, P. O. Andersson, W. Hk, T. Rindzevicius, M. S. Schmidt, V. R. Soma, S. Xu, Y. Li, A. Boisen, *ACS Sens.* **2017**, *2*, 198.

[70] Z. M. Jin, W. Gu, X. B. Shi, Z. K. Wang, Z. Q. Jiang, L. S. Liao, *Adv. Opt. Mater.* **2014**, *2*, 588.

SUPPORTING INFORMATION

Additional supporting information may be found online in the Supporting Information section at the end of the article.

How to cite this article: Byram C, Moram SSB, Soma VR. Surface-enhanced Raman scattering studies of gold-coated ripple-like nanostructures on iron substrate achieved by femtosecond laser irradiation in water. *J Raman Spectrosc*. 2019;1–11. https://doi.org/10.1002/jrs.5617